Available online at www.sciencedirect.com

SciVerse ScienceDirect

Acta Materialia 60 (2012) 4768–4779

Acta MATERIALIA

www.elsevier.com/locate/actamat

Prediction of post-dynamic austenite-to-ferrite transformation and reverse transformation in a low-carbon steel by cellular automaton modeling

Chengwu Zheng [a], Dierk Raabe [a,*], Dianzhong Li [b]

[a] Max-Planck Institut für Eisenforschung, Max-Planck-Straße 1, Düsseldorf 40237, Germany
[b] Institute of Metal Research, Chinese Academy of Sciences, Wenhua Road 72, Shenyang 110016, China

Received 28 March 2012; received in revised form 2 June 2012; accepted 4 June 2012

Abstract

The post-dynamic transformation that takes place during the subsequent isothermal holding for the case when dynamic strain-induced transformation (DSIT) from austenite to ferrite occurs during hot deformation is investigated by cellular automaton modeling. The simulation provides a better understanding of carbon diffusion in retained austenite and the resulting microstructure evolution during the post-dynamic transformation. The predictions reveal that continuing transformation from retained austenite to ferrite and the reverse transformation can occur simultaneously in the same microstructure during post-deformation isothermal holding owing to the locally acting chemical equilibrium conditions. Competition between forward and reverse transformation exists during the early stage of post-dynamic heat treatment. It is also revealed that increasing the final strain of DSIT might promote the reverse transformation, whereas the continuous austenite-to-ferrite transformation yields a diminishing effect. The influence of the DSIT final strain on the grain size of ferrite and the characteristics of the resultant microstructure is also discussed.

Keywords: Strain-induced transformation; Post-dynamic transformation; Cellular automaton; Modeling; Low-carbon steel

1. Introduction

A primary goal in steel design is to refine the ferrite grain size, as this is a mechanism that can simultaneously improve strength and toughness. Hence, specific emphasis has been placed on the large-scale design of ultrafine-grained steels [1–3]. In recent years, a number of techniques and methods have been developed to produce ultrafine-grained steels with a ferrite grain size of around 1 μm [4–11]. Among the various approaches, the novel technique of dynamic strain-induced transformation (DSIT) [1,12] from austenite to ferrite has received much attention owing to its capability of producing ultrafine ferrite (UFF) microstructures with grain sizes that typically fall into the 1–3 μm range [11–21]. In DSIT, the UFF microstructure is achieved by heavy deformation of the undercooled, metastable austenite just above the transformation start temperature (Ar3) without using high levels of alloying. In general, the concurrent deformation and phase transformation is believed to be necessary for UFF microstructure production in the DSIT process. Owing to its conceptual simplicity and efficiency for grain refinement, and the associated improvement in strength and toughness, the DSIT mechanism has been the subject of extensive investigations [11–26].

Commonly, a typical DSIT schedule consists of a reheating step to form a desired austenite grain size and subsequent cooling to a deformation temperature between the Ae3 and Ar3 temperatures (the equilibrium and empirical austenite to ferrite transformation temperature, respectively). Specific deformation (e.g. deformation mode and

* Corresponding author. Tel.: +49 211 6792 340; fax: +49 211 6792 333.
E-mail address: raabe@mpie.de (D. Raabe).

1359-6454/$36.00
http://dx.doi.org/10.1016/j.actamat.2012.06.007

level) is then applied to achieve UFF. Suitable post-deformation treatment (e.g. controlled cooling) is also generally included to preserve the UFF microstructure obtained via DSIT when the deformation is interrupted. During the DSIT process, the time available for phase transformation is usually insufficient to fully complete the transformation from austenite to DSIT ferrite. The unstable retained austenite can continue transforming into ferrite. Such post-dynamic transformation (post-DT) influences the final microstructure of the product significantly. Just like the metadynamic recrystallization [27], post-DT can start immediately after deformation without any incubation period as ferrite nuclei are already present in the material. The transformation kinetics can also differ from that of conventional γ–α transformation or DSIT.

Despite the considerable importance of UFF design strategies, only a few investigations have focused on post-DT. Recently, Sun et al. [28] investigated the microstructural evolution and kinetics of the isothermal post-DT after compression deformation in a low-carbon steel using both dilatometry and optical microscopy. However, the focus was centered on the development of a quantitative dilatometric method for the measurement of the DSIT ferrite fraction [29]. Due to the limitations of the experimental methods they used, Sun et al. were unable to improve their understanding of the post-DT mechanism significantly. It still remains unclear how ferrite growth were controlled through the post-deformation process.

With the recent development of mesoscale microstructure-based transformation models [30], simulations can now provide deeper insight into the mechanism of the austenite–ferrite transformation and its morphological complexity. Various mesoscopic methods are conceivable, e.g. the cellular automaton (CA) [31–36], the Monte Carlo [37,38] and the phase field models [39–42].

Recently, the present authors developed an integrated CA model to simulate DSIT in low-carbon steels [43,44]. In that work the nucleation of DSIT ferrite and the associated carbon diffusion behavior during DSIT were addressed. The refinement mechanism of the DSIT ferrite can also be studied. The present work is built on the previous work of DSIT modeling, focusing on the numerical simulation of microstructure evolution during post-DT after DSIT. In this work, a modified CA model is developed to jointly predict the metallurgical mechanisms of solute diffusion, interface migration and grain coarsening which pertain to the post-DT mechanism. In modeling this transformation, the simulated results of DSIT, including the morphology of grains, distribution of phases and solute concentration field, are input as the initial conditions for the following post-DT simulation. Specifically, this model takes into account the effect of local solute redistribution on the migration of the γ/α interfaces, which allows both the continuing transformation from austenite to ferrite and the reverse transformation to be studied. The influence of the DSIT final strain on the transformation kinetics and microstructure evolution is also obtained by the model.

2. Model concept

2.1. Growth of ferrite grains

When deformation is interrupted after DSIT, the strain-induced ferrite grains can grow continuously during the subsequent post-deformation holding period. Different from conventional grain-coarsening, this mechanism of the movement of the γ/α interface can be referred to as "transformation growth". The driving force comes from the difference in free energy between the two phases. In our model, the kinetics of ferrite growth during post-DT is described as a mixed-mode process governed both by carbon diffusion and by the γ/α interface mobility. The transformation associated with the γ/α interface motion is described by a free boundary problem for carbon diffusion in austenite and the dynamics of the moving interface. The kinetics of the γ/α interface is determined by

$$V_{\alpha\gamma} = M_{\alpha\gamma} F \tag{1}$$

where $V_{\alpha\gamma}$ is the velocity of γ/α interface and $M_{\alpha\gamma}$ is the effective mobility of γ/α interface, which includes the structural influence on the interface mobility, such as incoherence, the set-up of stresses and solute drags. It can be described, as per Loginova et al. [45], as:

$$M_{\alpha\gamma} = M_0 \exp\left(-\frac{Q_{\alpha\gamma}}{RT}\right) \tag{2}$$

where M_0 is the pre-exponential factor of the interface mobility, $Q_{\alpha\gamma}$ is the activation energy for boundary migration, R is the universal gas constant (8.314 J mol^{-1} K^{-1}) and T is the absolute temperature (in K).In DSIT, the driving force for interface migration, F is provided both by the chemical driving force, F_{chem}, that is associated with the transformation and by the stored deformation energy, E_d,

$$F = F_{chem} + E_{\mathrm{d}} \tag{3}$$

The chemical driving force for the γ/α interface migration, F_{chem}, can be derived from Svoboda et al. [46]:

$$F_{chem} = \mu^{\gamma}_{Fe} - \mu^{\alpha}_{Fe} \tag{4}$$

where μ^{γ}_{Fe} and μ^{α}_{Fe} are the chemical potentials of iron in austenite and ferrite, respectively, determined by the local carbon concentration on either side of the γ/α interface. The chemical potentials of iron in austenite and ferrite phases are calculated using the regular solute sublattice model [47] in the simulation.

During the post-dynamic holding, the stored deformation energy E_d is released dramatically due to recovery. The evolution of the stored energy $E_d(t)$ with soaking time t is given as following [48],

$$E_d(t) = \left[E_d(t_0)^{1/2} - C_0 \mu_i^{-1/2} kT \ln\left(1 + \frac{t}{\tau_0}\right)\right]^2 \tag{5}$$

where $E_d(t_0)$ is the initial stored energy of deformation which comes from the previous DSIT simulation [44], t_0 is the time when recovery starts, C_0 is a combined fitting

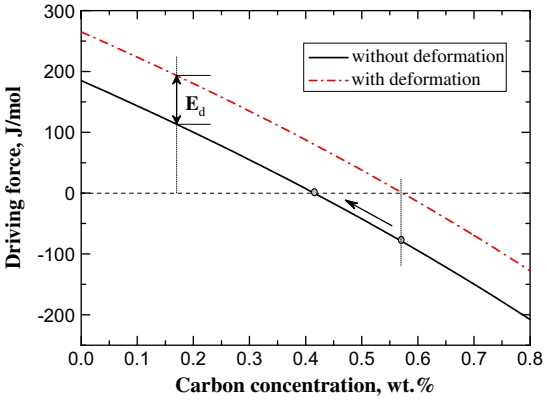

Fig. 1. Driving force for γ–α transformation as a function of carbon concentration in low-carbon steel at 780 °C.

parameter, μ_i is the shear modulus of the material ($i = \alpha, \gamma$) and k is the Boltzmann constant. Recovery is assumed to occur from the start of the post-deformation soaking, i.e. $t_0 = 0$ s. τ_0 is a time constant, which was set at 1 s in the present simulation.

Fig. 1 shows the typical calculated driving force for the γ/α interface migration at the given temperature of $T = 780$ °C. It can be seen that the driving force decreases gradually with increasing carbon concentration in austenite. The driving force falls to zero when the carbon concentration in austenite approaches its equilibrium value. The motion of the γ/α interface then ceases. At 780 °C, the equilibrium carbon concentration in austenite is 0.41 (wt.%). In DSIT, the driving force is increased markedly due to the effect of the deformation stored energy. The equilibrium carbon concentration is also increased accordingly. However, with the release of the deformation stored energy during isothermal holding, this concentration value becomes supersaturated in the subsequent post-DT. The driving force for the γ/α interface motion then becomes negative, which indicates that the induced ferrite should transform back to austenite at the γ/α interface. This mechanism is referred as "reverse transformation". The schematic illustration of the reverse transformation occurred at the γ/α interface can be seen in Fig. 2.

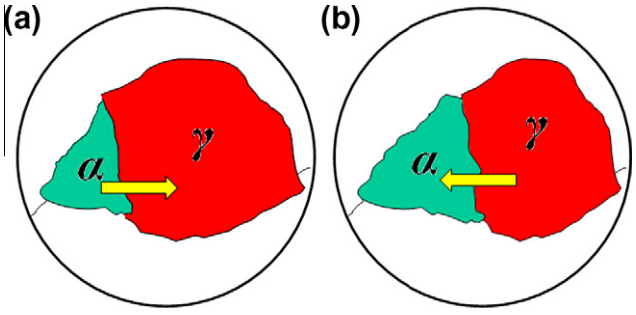

Fig. 2. Schematic illustrations of γ/α interface migration during the transformation from austenite to ferrite (a) and the reverse transformation (b).

Carbon diffusion is occurring during the entire process. Because the carbon solubility in ferrite is much smaller than in austenite, carbon diffusion in ferrite is neglected here. The carbon diffusion in austenite is described by

$$\frac{\partial c}{\partial t} = \nabla \cdot (D_\gamma \nabla c) \tag{6}$$

where c is the carbon concentration (wt.%) and t is the time. D_γ is the carbon diffusion coefficient in austenite, which can be calculated using the following relation [49]:

$$D_\gamma = D_0 \exp[-1.6c - (37000 - 6000c)/RT] \tag{7}$$

where D_0 is the pre-exponential factor of the carbon diffusion.

2.2. Ferrite grain coarsening behind the transformation fronts

During DSIT, ferrite grain layers are continually formed close to the γ/α interface and gradually extend into the austenite interior [44]. This nucleation mode can not only lead to a higher nucleation density, but also facilitate the hard impingement among the neighboring ferrite grains. The ferrite grains impinge upon each other directly in DSIT as the phase transformation proceeds. At this stage, the ferrite grain boundaries rarely remain in their local mechanical equilibrium after impingement but, rather, are driven further away by the curvature [50,51] during subsequent post-deformation holding. According to Burke and Turnbull [50], the velocity of a grain boundary segment driven by the curvature can be expressed by

$$V_{\alpha\alpha} = M_{\alpha\alpha} P \tag{8}$$

where $M_{\alpha\alpha}$ is the grain boundary mobility between ferrite grains and P is the driving force for grain boundary mobility. The driving force for boundary motion P can be expressed by

$$P = \gamma\kappa \tag{9}$$

where γ is the ferrite grain boundary energy and κ is the curvature of the α/α grain boundary. Up to 15° misorientation, the grain boundary energy γ can be calculated by the Read–Shockley equation [52]:

$$\gamma = \gamma_m \left(\frac{\theta}{\theta_m}\right)\left[1 - \ln\left(\frac{\theta}{\theta_m}\right)\right] \tag{10}$$

where θ is the grain boundary misorientation, and γ_m and $\theta_m = 15°$ are the boundary energy and misorientation when the grain boundary becomes a high angle boundary. Beyond 15°, we assume a constant value for the grain boundary energy.Several approaches have been suggested to calculate the interface curvature in lattice-based models [53–56]. In the current simulation, an approach known from solidification [56] is adopted to calculate the grain boundary curvature:

$$\kappa = \frac{A}{C_{cell}} \frac{Kink - N_i}{N + 1} \tag{11}$$

where C_{cell} is the cell size in the CA model, $A = 1.28$ is a topological coefficient, $N = 18$ is the number of the first and second nearest neighbors for a hexagonal lattice, N_i is the number of cells within the neighborhood belonging to grain i, and $Kink = 9$ is the number of cells within the neighborhood belonging to grain i for a flat interface ($\kappa = 0$). The topological considerations behind this model can be found in Figs. A1–A3 in Ref. [56].

2.3. The CA model

The CA model used for the current post-DT simulation is a modification of the approach developed in our previous studies [43]. In this formulation, the spatial system is discretized into a two-dimensional (2-D) regular hexagonal lattice. Each cell represents a volume of real material with a distinct phase, solute content and orientation indicator. The neighbors of a cell are defined by Von Neumann's rule, which considers the six nearest cells. In order to describe the microstructural evolutions during the post-deformation isothermal holding, six state variables are assigned to each CA node. These are: (i) the phase state, which denotes whether the cell is ferritic, austenitic, or contains a γ/α interface; (ii) the orientation variable, which is assigned an integer identifier representing its crystallographic orientation; (iii) the carbon concentration; (iv) the ferrite transformation fraction variable, f_α, representing the ferrite fraction transformed; (v) the austenite transformation fraction variable, f_γ, quantifying the austenite fraction transformed; and (vi) the fraction variable, f, used for the motion of the boundary segment within an α/α boundary cell.

The kinetics of the automaton is realized by synchronously updating the state variables for all lattice cells in each time step.

A deterministic transformation rule is applied to determine the changing state of each CA cell. For the cell (i,j), in which the status variable belongs to the moving interface, the moving distance of the interface in a single time step, Δt, is described as:

$$l^t_{i,j} = \int_t^{t+\Delta t} v dt \tag{12}$$

where v is the velocity of the boundary movement. The indices (i,j) denote the coordinate of the selected interface cell. The transformation fraction in (i,j), $f^t_{h,k}$, is then calculated by:

$$f^t_{i,j} = l^t_{i,j}/L_{CA} \tag{13}$$

where L_{CA} is the distance between two neighboring cells. If the accumulated value of the transformation fraction variable is greater than 1.0, the interface cell switches into the new state from the neighboring cells belonging to the corresponding growing grain.

Details about the implementation of the transition rules for austenite–ferrite transformation or DSIT in carbon steel are provided in Refs. [34,44]; only the novel key points for the current post-DT simulation procedure are outlined here:

(1) During post-DT, further nucleation of ferrite is not considered during the entire isothermal holding time. All ferrite nuclei appeared during deformation through the DSIT mechanism.
(2) The motion of the γ/α interface is highly correlated with the local carbon concentration. Whether the γ/α interface moves from the retained austenite into the ferrite or from DSIT ferrite into austenite is determined by the local driving force for interface migration. Hence, in the simulation of grain growth, the chemical driving force, F_{chem}, is first calculated for each γ/α interface cell according to the local carbon concentration.

When $F_{chem} \geqslant 0$, the γ/α interface moves from austenite into ferrite. The resulting interface velocity and the ferrite transformation fraction, f_α, inside the interface cells are calculated using Eqs. (1) and (13), respectively. If f_α is not below 1, the phase state of the cell switches to ferrite and all of its neighboring austenite cells change into γ/α interface cells. The excess carbon atoms are rejected into these surrounding interface cells. The carbon atoms diffuse into the surrounding austenite regions at a rate given by Fick's second law, which can be solved numerically using a finite volume method.

In contrast, when $F_{chem} < 0$, the γ/α interface shifts from ferrite to austenite, which implies a reverse transformation of the induced ferrite back to austenite. In this case, the phase state of the interface cell changes into austenite.

(3) Curvature-driven grain coarsening is assumed to only occur between the ferrite grains after the moving fronts impinge on each other. For the boundary cell on the α/α interface, the curvature is calculated by Eq. (11). The velocity of the corresponding boundary and the direction of the motion can then be determined. The fraction of the boundary segment within the boundary cell is calculated according to Eqs. (12) and (13). Finally, the crystallographic orientation of a boundary cell is reassigned when the boundary migrates through it ($f \geqslant 1$).

3. Details of the post-DT simulation

A plain low-carbon steel with a chemical composition (wt.%) of 0.17C, 0.27Si and 0.71Mn is selected for this study, according to the experimental data used in Refs. [28,29]. The transformation temperature Ae3 is calculated as 835 °C by Thermo-Calc. The corresponding thermomechanical processing schedule used for the post-PT study is shown schematically in Fig. 3. The specimen is first heated up to 1000 °C and held at that temperature for 3 min to obtain a single-phase austenite microstructure. It is then

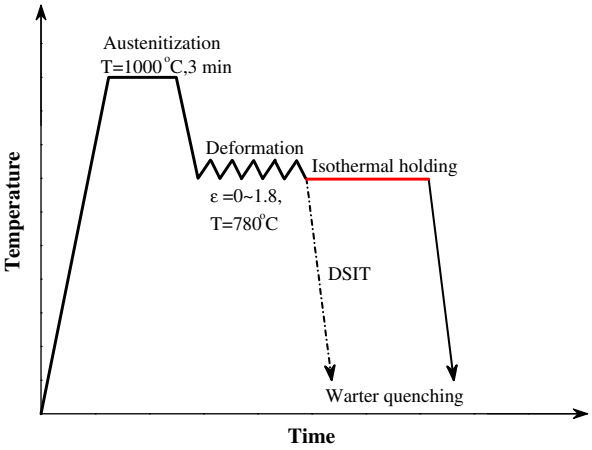

Fig. 3. Schedule of thermomechanical processing used in the post-PT simulation.

cooled to the deformation temperature of 780 °C and subjected to a uniaxial compression series consisting of logarithmic straining steps of $\varepsilon = 0$–1.8 at a strain rate of 10 s^{-1}. During the deformation at the given temperature, DSIT occurs, which leads to ultrafine-grained ferrite in this material. After the deformation, the specimen is held isothermally at the soaking temperature (780 °C) until the post-DT is complete.

In the current simulation, we use a 330 × 240 2-D lattice to discretize the simulated domain, representing a physical domain of 132 μm × 96 μm in the real material. The initial single austenite microstructure is created according to a normal grain growth process, with an average grain size of 15 μm radius. The dynamic strain-induced transformation from austenite to ferrite is simulated using the previously developed CA model [43,44]. Details about the DSIT modeling can be found in Refs. [43,44]. The simulation results of DSIT are then used as the starting state for the subsequent post-dynamic simulation, including the morphology of grains, the distribution of phases and the solute concentration field. The post-DT is not a distinctly separated process; rather, it is a continuing transformation of the deformation-induced ferrite formed during straining. Fig. 4 describes the simulated DSIT microstructure and the associated carbon concentration field (wt.%) at the final strain of $\varepsilon_0 = 0.8$, which is also used as the input of the starting microstructure in the subsequent post-DT modeling. In the simulated microstructure, the white regions are retained austenite phases and the colored areas are DSIT ferrite grains with different orientations. Different grains are separated by black lines (ferrite grain boundaries).

In this paper, grain size is defined by an equivalent grain radius R_i according to:

$$R_i = \sqrt{\frac{A_i}{\pi}} \tag{14}$$

where A_i is the area of ferrite grain i, which can be calculated by summing the number of cells of each ferrite grain included. The average ferrite grain size $\langle \overline{R} \rangle$ is calculated as

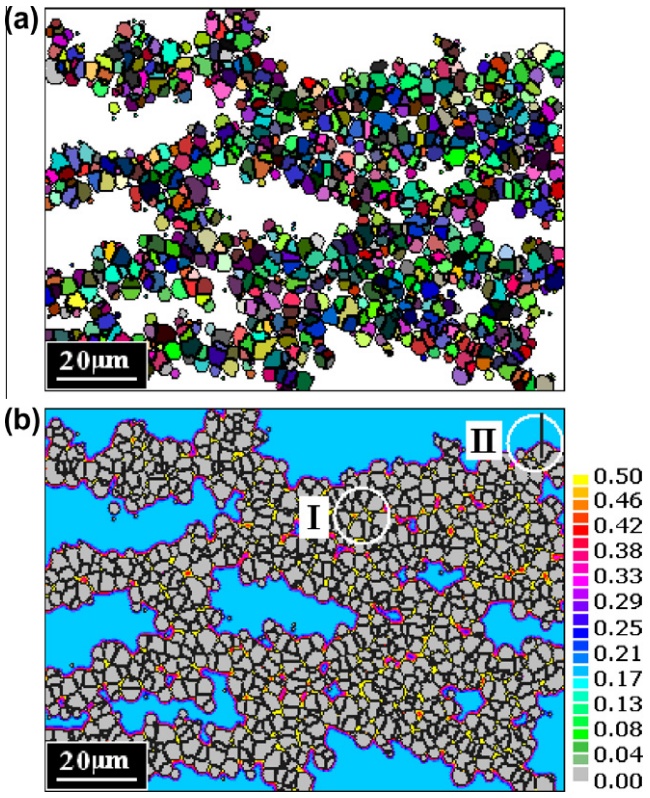

Fig. 4. The DSIT microstructure (a) and carbon concentration field (b) at the final deformation of $\varepsilon_0 = 0.8$, which are also used as input for the subsequent post-DT simulation. The different colorful areas in the microstructure are the DSIT ferrite grains with different crystallographic orientations; the white regions are retained austenite phase. (For interpretation of the references to colour in this figure legend, the reader is referred to the web version of this article.)

$$\langle \overline{R} \rangle = \frac{(\sum_{i=1}^{N_\alpha} R_i)}{N_\alpha} \tag{15}$$

where N_α is the total number of ferrite grains in the system. The key parameters used in the modeling are listed in Table 1.

4. Simulation results and discussion

Fig. 5a shows the simulated kinetics of ferrite formation during post-DT when the DSIT final strain ε_0 is 0.8. The volume fraction of ferrite decreases rapidly during the early stage of post-DT. This indicates that a fast reverse transformation occurs from the induced ferrite back to austenite at this stage. This transformation depends strongly on the local distribution of the carbon concentration within the simulation domain as the drive towards local chemical equilibrium determines the driving force for it. The associated carbon composition field set as input for the post-DT simulation is shown in Fig. 4b. We observe that the carbon concentration is distributed very heterogeneously. As mentioned earlier [44], only short-range carbon diffusion can take place during DSIT owing to time constraints. The carbon atoms are concentrated within a narrow but sharp

Table 1
Key parameters used in simulations [44,49].

M_0 (mmol J^{-1} s^{-1})	$Q_{\alpha\gamma}$ (kJ mol^{-1})	D_0 (m^2 s^{-1})	γ_m (J m^{-2})	μ_α (GPa)	μ_γ (GPa)	C_0 (m^{-3})
0.5	147	4.7×10^{-5}	0.56	32	50	7.8×10^{28}

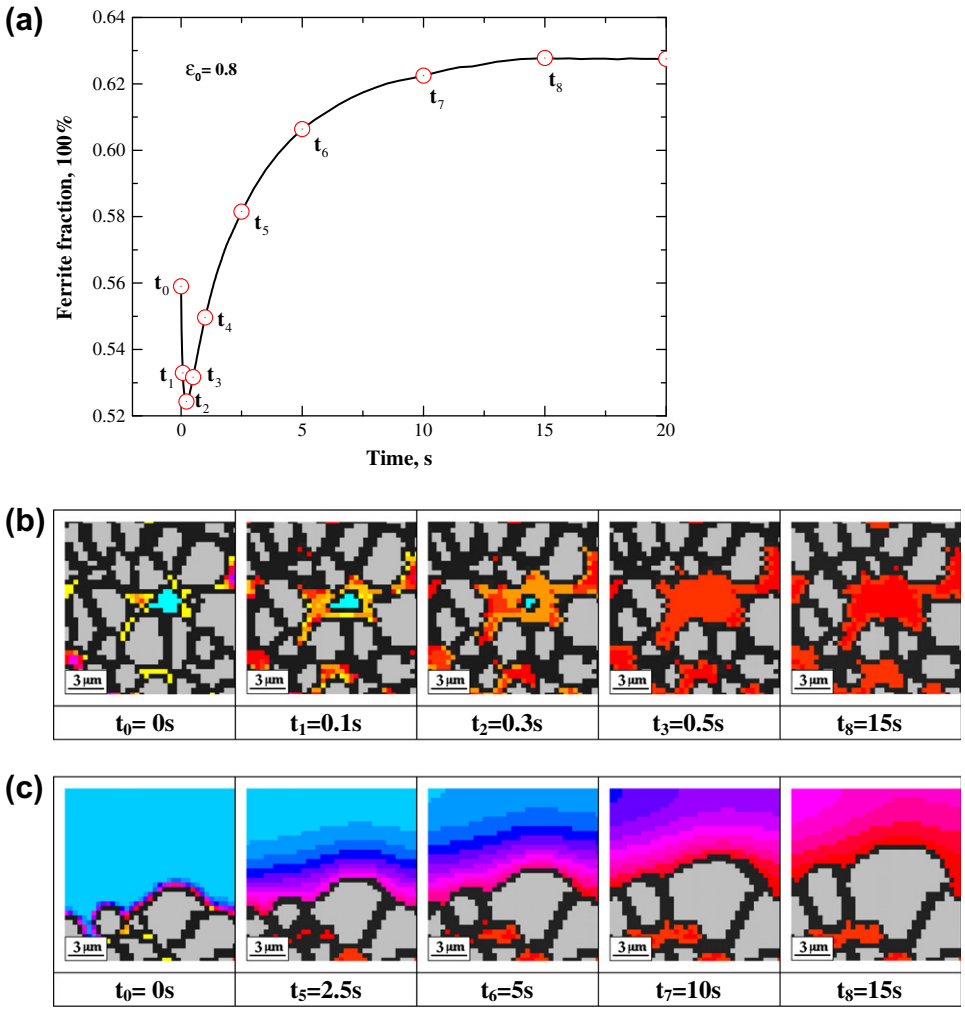

Fig. 5. Simulated transformation kinetics of ferrite during post-DT at the DSIT final strain of 0.8 (a); snapshots at different times of the carbon concentration field in reverse transformation (b) and continuing austenite-to-ferrite transformation (c) in the selected regions in Fig. 4. In these pictures, the black lines represent grain boundaries. The carbon-poor areas where the carbon concentration is lower than 0.022 wt.% indicate the ferrite phase.

layer in front of the moving γ/α interface, while the regions far away from the γ/α interface retain their initial austenitic carbon concentration. Furthermore, in DSIT, continuous ferrite formation in front of the γ/α interface facilitates the soft impingement (i.e. the overlapping of the carbon concentration fields) among the neighboring ferrite grains. The rapid accumulation of carbon atoms at the transformation interface front decreases the driving force for the γ/α interface migration, resulting in the formation of isolated islands of austenite with high carbon concentrations surrounded by fine ferrite grains. In these austenitic regions, the motion of the γ/α interface is fully retarded due to the high carbon enrichment during DSIT. However, with the release of the deformation energy during the subsequent isothermal holding, this concentration value changes, becoming supersaturated compared to the equilibrium concentration. The driving force for the motion of the γ/α interface becomes negative under this circumstance, indicating that reverse migration for the γ/α interface should take place from ferrite back to austenite.

Fig. 5b shows snapshots of the local carbon concentration field as a specific case of the reverse transformation in the selected zone "I" in Fig. 4b. We observe that the marked ferrite grain is indeed shrinking gradually owing to the reverse transformation. The γ/α interface segments continue to move from austenite to ferrite, until the ferrite grain finally vanishes completely. Carbon redistribution within the austenite accompanies the transformation.

When the carbon concentration approaches its final equilibrium value, the γ/α interface motion stops and the reverse transformation ceases.

In a previous study, Luo et al. [57] also observed the retransformation phenomenon of ferrite to austenite in a C–Mn steel during isothermal relaxing after deformation at 775 °C. They suggested that the difference in the softening rate of the stored energy in the two phases changes the phase equilibrium and thus leads to the observed α–γ retransformation. The current results reveal another reasonable explanation for the mechanism of the reverse transformation during the post-dynamic process.

At the end of DSIT, vary narrow carbon-rich regions form within the austenite phase near the moving γ/α interface. There exists a noticeable concentration gradient within these local regions, as shown in Figs. 4b and 6. Driven by this concentration gradient, carbon atoms gradually diffuse from the interface into the austenite interiors during the subsequent isothermal holding period, and this decreases the carbon concentration at the moving γ/α interface. When the carbon concentration in austenite is less than 0.41 (wt.%), the driving force for interface mobility from austenite to ferrite should change to positive. However, the interface exhibits no noticeable movement due to the relatively low driving force and limited transformation time during the early stage, which indicates that the continuous growth of the DSIT ferrite should be suppressed temporarily owing to a solute drag effect. This mechanism, combined with the effect of the reverse transformation, should be responsible for the rapid decrease in the transformation kinetics of ferrite observed in Fig. 5a. Yang et al. [58] in fact previously reported that this type of partial retransformation from DSIT ferrite into austenite occurred during holding at a temperature between Ae3 and Ar3.

As the isothermal holding progresses further, the carbon atoms on the γ/α interface diffuse into the austenite grain interior by long-range diffusion. As a result, the ferrite grains grow steadily until the carbon concentration in the retained austenite has increased to the equilibrium value, as shown in Fig. 6. A much clearer demonstration of this process can be found in Fig. 5c, which presents snapshots of the simulated concentration maps within the selected region "II". When the continuing transformation of retained austenite to ferrite is faster than the reverse transformation, the volume fraction of ferrite rises again during subsequent holding, as indicated in Fig. 5a. This implies that competition exists between the austenite–ferrite transformation and the reverse transformation during post-DT after DSIT. The overall transformation kinetics can be understood as a dynamic equilibrium between these two mechanisms.

Fig. 7 shows the change in the ferrite fraction as a function of soaking time during post-DT at different DSIT final strains. It is seen that a larger strain introduced more ferrite transformed at the end of DSIT ($t = 0$ s). During the early stage of the subsequent post-DT, the transformation kinetics exhibits no obvious reverse transformation if the DSIT final deformation is not sufficient. The remaining austenite transforms into ferrite continuously and gradually until it reaches the final thermodynamic equilibrium. However, with increasing DSIT final deformation, reverse transformation is seen to be promoted. In contrast, the continuing transformation from retained austenite to ferrite is suppressed. When the DSIT final deformation is raised up to $\varepsilon_0 = 1.6$, the continuing γ-to-α transformation becomes unnoticeable.

Figs. 8 and 9 show the changes both in the transformation microstructure and in the carbon concentration field during post-DT at DSIT final strains of $\varepsilon_0 = 0.35$ and $\varepsilon_0 = 0.8$, respectively. In the images on the right-hand side, the carbon-depleted areas where the carbon concentration is below 0.02 wt.% indicate the occurrence of the ferrite phase. It should be noted that further ferrite nucleation is not considered during post-dynamic isothermal holding. The nucleation situation of ferrite by DSIT, however, affects the following post-DT. When DSIT was interrupted at the small deformation of $\varepsilon_0 = 0.35$, with a small group of fine ferrite grains being formed along the prior austenite grain boundaries in a low volume fraction. In this case,

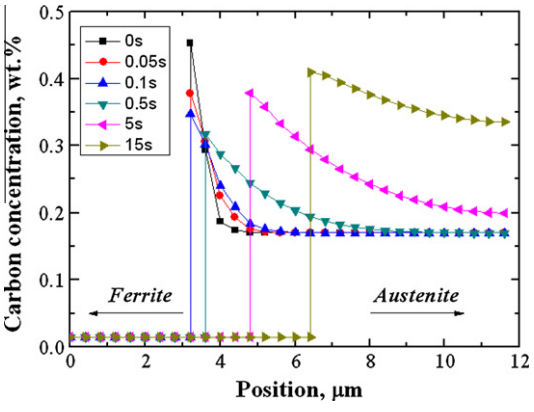

Fig. 6. Variation in the carbon concentration along the black line (starting from the bottom) in Fig. 4b at different soaking times.

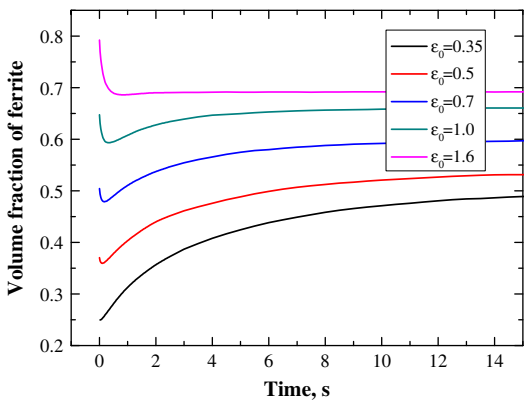

Fig. 7. Simulated transformation kinetics of ferrite during the post-DTs at different DSIT final deformations.

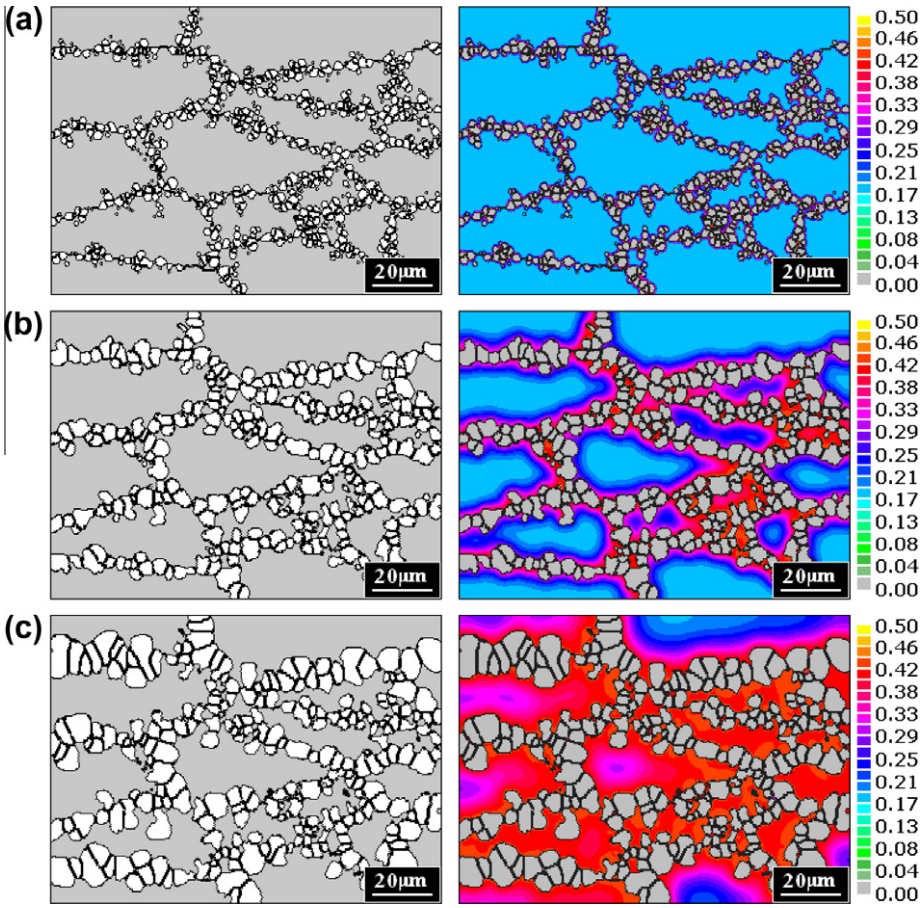

Fig. 8. Simulated microstructure and carbon concentration field (wt.%) during post-DT at different soaking times, (a) $t = 0$ s, (b) $t = 2.5$ s and (c) $t = 15$ s, at the DSIT final strain of 0.35. The black lines in the figures indicate the grain boundaries. The white areas in the left images are the ferrite phase and the gray regions are the retained austenite phase.

the carbon concentration in the carbon-rich region on the γ/α interface is not high enough to trigger the reverse transformation. The ferrite grains are able to grow freely into the austenite phase. When the deformation rose to $\varepsilon_0 = 0.8$, more DSIT ferrite was formed in rafts and covered the original austenitic area behind the moving γ/α interface. Soft impingements easily occurred among these fine ferrite grains to form a localized microstructure of isolated carbon-enriched austenite islands surrounded by fine ferrite grains. Thus, reverse transformation is likely to take place more easily in this situation during the subsequent isothermal holdings. Further growth of the DSIT ferrite could nevertheless take place, because there are large areas of retained austenite in the grain interior. These zones provide favorable regions for long-range carbon diffusions. As a result, the ferrite grains adjacent to these austenitic regions are seen to clearly grow during subsequent post-DT, which would produce more heterogeneous size distributions in ferrite grains than the initial input.

From the above arguments, we expect that, when the prior austenite is completely replaced by the mixed microstructure of small-sized austenite islands and fine DSIT ferrite at much larger DSIT final deformation, continuing growth of the DSIT ferrite grains would be restricted owing to the lack of favorable spaces for long-range carbon diffusion. Hence, a pronounced increase in the ferrite fraction in the transformation kinetics would not be detectable, as seen in Fig. 7, when the DSIT final deformation is increased to $\varepsilon_0 = 1.6$. On the contrary, the reverse transformation becomes preferential.

These results suggest that the transformations during the post-dynamic isothermal holding are strongly affected by the DSIT final strain: it determines which occurs preferentially for the continuing transformation from retained austenite to ferrite and the reverse transformation until the final thermodynamic equilibrium is reached. However, it should be noted that, although significant differences in Fig. 7 are observed in the ferrite volume fraction after 15 s of isothermal holding at different DSIT final strains, theoretically these differences will eventually disappear; i.e., given enough time, the material should reach the equilibrium fraction at this annealing temperature. This stage takes quite a long time to complete, as confirmed by experiments [28,29]. Modeling of the final equilibrium is not attempted in the current simulation; instead, interest is focused on the microstructural changes at the initial stage of post-DT.

Fig. 10 describes the variations in average grain size of ferrite during the post-deformation isothermal holdings at

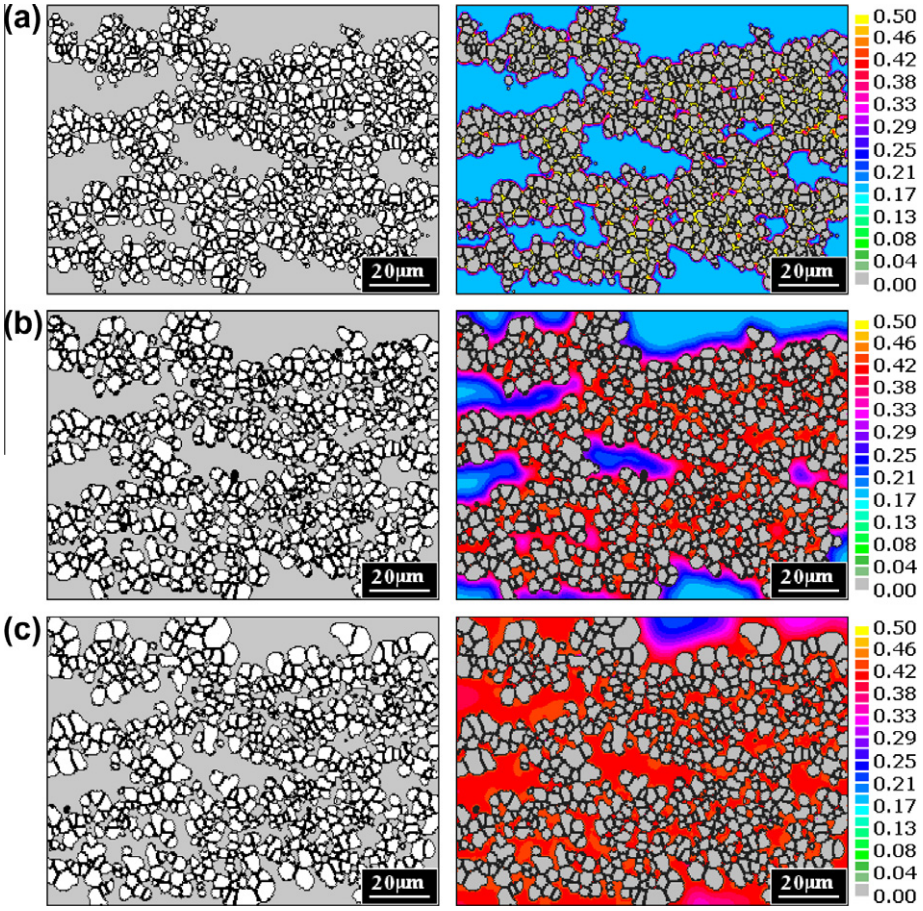

Fig. 9. Simulated microstructure and carbon concentration field (wt.%) during the post-DT at different soaking times, (a) $t = 0$ s, (b) $t = 2.5$ s and (c) $t = 15$ s, at the DSIT final strain of 0.8. The black lines in the figures indicate the grain boundaries. The white areas in the left images are the ferrite phase and the gray regions are the retained austenite phase.

the two different DSIT final strains of $\varepsilon_0 = 0.35$ and $\varepsilon_0 = 0.8$. It can be seen that further growth of the ferrite grains is more evident at the smaller DSIT final deformation. A similar phenomenon is found in the simulated microstructures in Figs. 8 and 9. In post-DT after DSIT, grain coarsening plays an import role in affecting the ferrite grain size. Compared with "transformation growth" (i.e. into austenite grains), grain coarsening is the displacement of the α/α interface after the ferrite grains impinge upon each other, where larger grains grow through the elimination of smaller ones. The driving force comes from the curvature of the grain boundaries. At the lower deformation of 0.35, "transformation growth" of the DSIT ferrite grains occurs very easily towards the large areas of retained austenite. Most of the remaining space is filled primarily by the growth, which would raise the overall average grain size markedly. Furthermore, it would also facilitate the coarsening of the enlarged grains by absorbing adjacent smaller ones. At the higher DSIT final strain of 0.8, however, a much larger population of fine ferrite grains is obtained at the end of the DSIT process. More importantly, these groups of fine grains extend to impinge in three dimensions [5]. The adjustment of α/α boundaries should be very slow in this condition, providing resistance of the fine DSIT ferrite against coarsening and growth. The small remaining austenite islands also retard the grain coarsening by pinning effect. This result suggests that increasing the DSIT deformation strain would help to preserve the fine ferrite grains obtained via DSIT by protecting them from coarsening in the subsequent post-dynamic treatment.

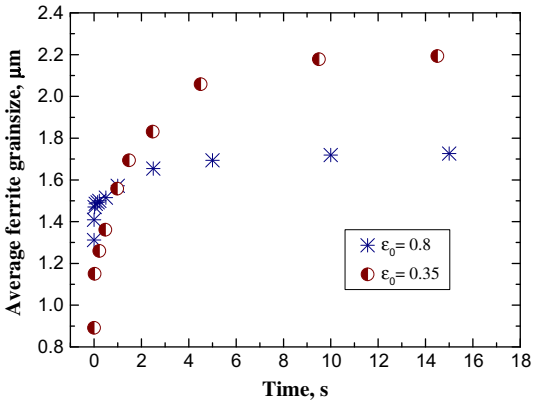

Fig. 10. Changes of the simulated average grain size of ferrite with soaking time at DSIT final strains of 0.35 and 0.8.

It should be pointed out that the discussions so far apply to only two dimensions, as they are based on 2-D simulations. There are potential limitations implied by the 2-D nature of the simulation. In 2-D simulation, grain edges and corners cannot be distinguished. Therefore, differences in ferrite nucleation caused by DSIT at these two locations cannot be described. This could render slight differences in the 2-D transformation kinetics of both DSIT and post-DT from the corresponding 3-D results. In addition, diffusion occurs in different ways in the 2-D and 3-D simulations: during 2-D simulation, the carbon atoms diffuse within the considered section but cannot diffuse in the normal direction, and this influences the evolution of the local carbon concentration fields. Despite the limitations, however, the current 2-D simulation presents a good description of post-DT after DSIT.

The quality of the phase transformation simulation can be verified by comparing the micrographs and simulated

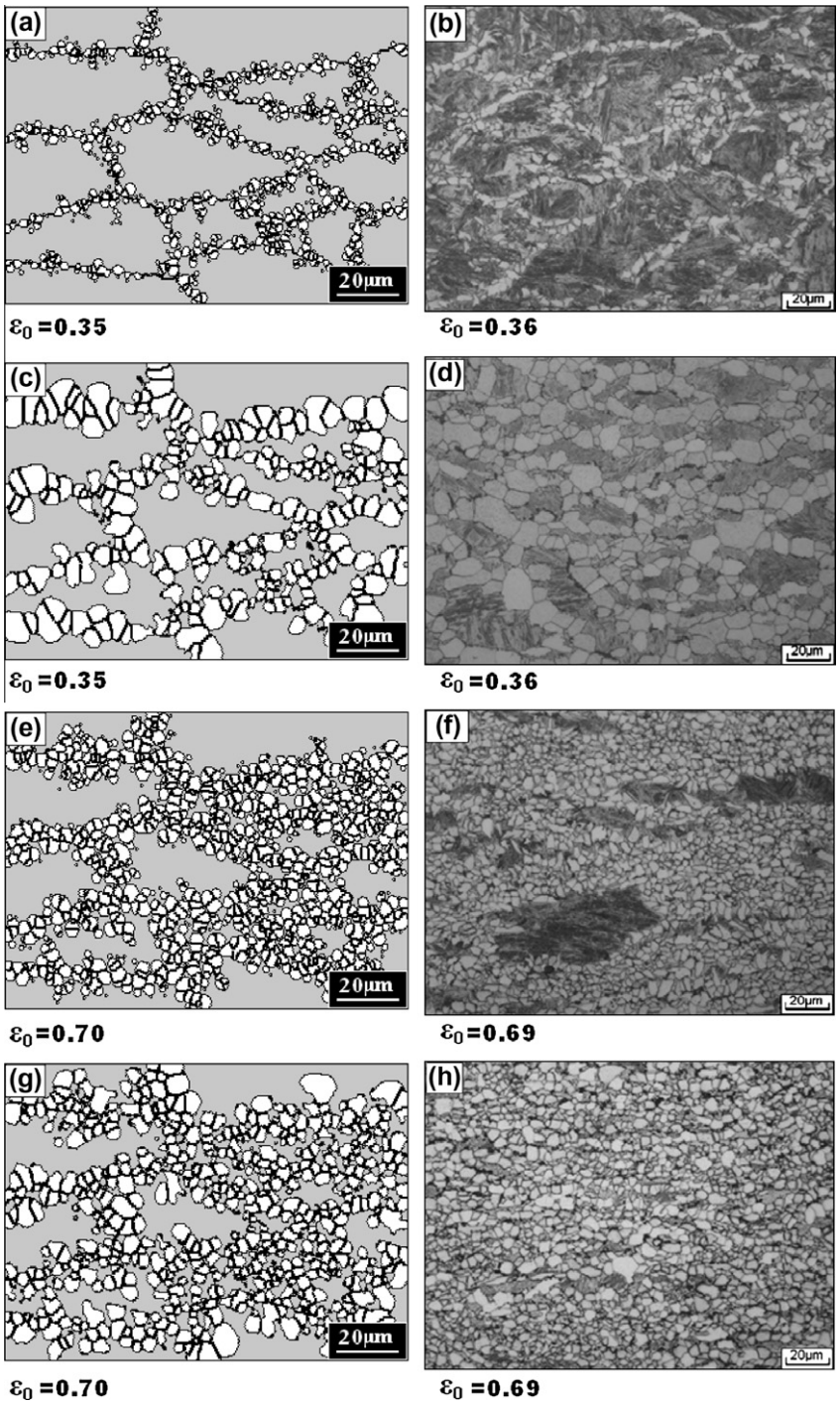

Fig. 11. Initial microstructures (a, b, e, f) and resultant microstructures (c, d, g, h) derived from the simulation (left) and from the optical micrographs (right) during the post-dynamic isothermal holdings of $T = 780$ °C at two DSIT final deformation levels (ε_0). In the simulated micrographs, ferrite is white and austenite is gray. In the optical micrographs, ferrite is light and martensite, which had been austenite before quenching, is dark.

microstructures. Fig. 11 shows the initial and resultant microstructures during post-DT at the two DSIT final deformation strain levels, as obtained both from the simulation and from metallography observations of water-quenched specimens by Sun et al. [29]. In the optical micrographs, the bright phase is ferrite and the dark is martensite, which was retained austenite before quenching. It is seen that the simulated phase arrangement and the grain structure resemble the metallographic results both in the initial and final microstructures at the two DSIT final strains. The same microstructural characteristics as previously discussed (Figs. 7–9) can be obtained in both simulated and observed microstructures. Thus, the present CA modeling could reproduce the post-DT after DSIT satisfactorily and also match the experimental results very well.

5. Conclusions

A CA modeling has been performed to investigate post-DT during isothermal holding for the case when DSIT occurred during deformation. In this model, the migration of the γ/α interface is dependent on the changing of local carbon concentrations, which permits both the continuing γ–α transformation and the reverse transformation to be simulated. The results of the simulation provide an insight into the variation in the carbon concentration field in retained austenite and the microstructure evolution during post-DT.

The results reveal that both the on-going austenite-to-ferrite transformation and the reverse transformation from DSIT ferrite to austenite might take place simultaneously during post-DT. There exists a competition between these two transformations during the early stage. When the DSIT final deformation is increased, the reverse transformation is promoted, whereas the austenite-to-ferrite transformation is reduced.

The results also show that ferrite grains tend to grow quite noticeably at small DSIT final deformations during post-DT. The UFF microstructure can be maintained more easily with a large volume fraction at larger DSIT deformations. This result indicates that greater deformation for DSIT would be more beneficial to preserving the UFF via DSIT during the subsequent post-dynamic processing. The predicted trends in ferrite grain size evolution as a result of various DSIT final deformations agree well with those from existing experimental findings.

Acknowledgement

C.W.Z. is grateful to the Alexander von Humboldt Foundation for the financial support.

References

[1] Weng YQ. Ultrafine grained steel. Beijing: Metallurgical Industry Press; 2008. p. 1.
[2] Howe AA. Mater Sci Technol 2000;16:1264.
[3] Song R, Ponge D, Raabe D, Speer JG, Matlock DK. Mater Sci Eng A 2006;441A:1.
[4] Song R, Ponge D, Raabe D, Kaspar R. Acta Mater 2005;53:845.
[5] Beladi H, Timokhinaa IB, Mukherjeea S, Hodgson PD. Acta Mater 2011;59:4186.
[6] Ohmori A, Torizuka S, Nagai K. ISIJ Int 2004;44:1063.
[7] Ueji R, Tsuji N, Minamino Y, Koizumi Y. Acta Mater 2002;50:4177.
[8] Valiev RZ, Langdon TG. Prog Mater Sci 2006;51:881.
[9] Saito Y, Utsunomiya H, Tsuji N, Sakai T. Acta Mater 1999;47:579.
[10] Ivanisenko Y, Lojkowski W, Valiev RZ, Fecht HJ. Acta Mater 2003;51:5555.
[11] Hodgson PD, Hickson MR, Gibbs RK. Mater Sci Forum 1998;284–302:63.
[12] Beladi H, Kelly GL, Hodgson PD. Int Mater Rev 2007;52:14.
[13] Yada H, Matsumura Y, Nakajima K. United States Patent No. 4,466,842, August 21, 1984.
[14] Yada H, Li CM, Yamagata H. ISIJ Int 2000;40:200.
[15] Hickson MR, Gibbs RK, Hodgson PD. ISIJ Int 1999;39:1176.
[16] Beladi H, Kelly GL, Shokouhi A, Hodgson PD. Mater Sci Eng A 2004;A367:152.
[17] Hodgson PD, Hickson MR, Gibbs RK. United States Patent No. 6,027,587, February 22, 2000.
[18] Choo WY, Um KK, Lee JS, Seo DH, Choi JK. In: International symposium on ultrafine grained steels, Fukuoka, Japan. Tokyo, Japan: ISIJ, The Iron and Steel Institute of Japan; 2001. pp. 2–9.
[19] Dong H. In: International Symposium on Ultrafine Grained Steels, Fukuoka, Japan. Tokyo, Japan: ISIJ, The Iron and Steel Institute of Japan, 2011. pp. 18–25.
[20] Mukhrejee K, Hazra SS, Militzer M. Metall Mater Trans A 2009;40A:2145.
[21] Priestner R, Al-Horr YM, Ibraheem AK. Mater Sci Technol 2002;18:973.
[22] Dong H, Sun XJ. Curr Opin Solid State Mater Sci 2005;9:269.
[23] Hurley PJ, Muddle BC, Hodgson PD. Metall Mater Trans A 2001;32A:1507.
[24] Hurley PJ, Muddle BC, Hodgson PD. Metall Mater Trans A 2002;33A:2985.
[25] Hong SC, Lim SH, Lee KJ, Shin DH, Lee KS. ISIJ Int 2003;43:394.
[26] Liu ZX, Li DZ, Lu SP, Qiao GW. ISIJ Int 2007;47:289.
[27] Humphreys FJ, Haterly M. Recrystallization and related annealing phenomena. 2nd ed. Oxford: Elsevier; 2004. p. 447.
[28] Sun XJ, Luo HW, Dong H, Liu QY, Weng YQ. ISIJ Int 2008;48:994.
[29] Sun XJ, Dong H, Liu QY, Weng YQ. Mater Sci Eng A 2008;487A:93.
[30] Raabe D. Philos Mag A 1999;79A:2339.
[31] Kumar M, Sasikumar R, Nair PK. Acta Mater 1998;46:6291.
[32] Zhang L, Zhang CB, Wang YM, Wang SQ, Ye HQ. Acta Mater 2003;51:5519.
[33] Kundu S, Dutta M, Ganguly S, Chandra S. Scripta Mater 2004;50:891.
[34] Lan YJ, Li DZ, Li YY. Acta Mater 2004;52:1721.
[35] Bos C, Mecozzi MG, Sietsma J. Comput Mater Sci 2010;48:692.
[36] Bos C, Mecozzi MG, Hanlon DN, Aarnts MP, Sietsma J. Metall Mater Trans A 2011;42A:3602.
[37] Tong MM, Li DZ, Li YY. Acta Mater 2005;53:1485.
[38] Xiao NM, Tong MM, Lan YJ, Li DZ, Li YY. Acta Mater 2006;54:1265.
[39] Huang CJ, Browne DJ, McFadden S. Acta Mater 2006;54:11.
[40] Militzer M, Mecozzi MG, Sietsma J, van der Zwaag S. Acta Mater 2006;54:3961.
[41] Takahama Y, Sietsma J. ISIJ Int 2008;48:512.
[42] Rudnizki J, Böttger B, Prahl U, Bleck W. Metall Mater Trans A 2011;42A:2516.
[43] Zheng CW, Li DZ, Lu SP, Li YY. Scripta Mater 2008;58:838.
[44] Zheng CW, Xiao NM, Hao LH, Li DZ, Li YY. Acta Mater 2009;57:2956.
[45] Loginova I, Odqvist J, Amberg G, Agren J. Acta Mater 2003;51:1327.
[46] Svoboda J, Fischer FD, Fratzl P, Gamsjager E, Simha NK. Acta Mater 2001;49:1249.

[47] Hillert M, Staffansson LI. Acta Chem Scand 1970;24:3618.
[48] Song X, Rettenmayr M. Mater Sci Eng A 2002;332A:153.
[49] Tibbetts GG. J Appl Phys 1980;51:4813.
[50] Burke JE, Turnbull D. Prog Met Phys 1952;3:220.
[51] Mullins WW. J Appl Phys 1956;27:900.
[52] Read W, Shockley W. Phys Rev 1950;78:275.
[53] Sasikumar R, Sreenivisan R. Acta Metall 1994;42:2381.
[54] Nastac L. Acta Mater 1999;47:4253.
[55] Jacot A, Rappaz M. Acta Mater 2002;50:1909.
[56] Kremeyer K. J Comput Phys 1998;142:243.
[57] Luo HW, Sietsma J, van der Zwaag S. Metall Mater Trans A 2004;35A:2789.
[58] Yang P, Fu WY, Cui FE, Sun ZQ. Acta Metall Sin 2000;37:601.